Available online at www.sciencedirect.com
SCIENCE DIRECT®

Journal of the European Ceramic Society 24 (2004) 717–723

www.elsevier.com/locate/jeurceramsoc

Reverse-microemulsion preparation and characterization of ultrafine orthorhombic $LiMnO_2$ powders for lithium-ion secondary batteries

Chung-Hsin Lu*, Hsien-Cheng Wang

Electronic and Electro-optical Ceramics Laboratory, Department of Chemical Engineering, National Taiwan University, Taipei, Taiwan, ROC

Received 10 January 2003; received in revised form 7 April 2003; accepted 15 April 2003

Abstract

Ultrafine orthorhombic $LiMnO_2$ (o-$LiMnO_2$) were successfully synthesized using a newly developed reverse-microemulsion (RμE) process. To prepare o-$LiMnO_2$ powders with a rock salt structure, precise control of the oxygen content in the heating atmosphere was required. Monophasic o-$LiMnO_2$ was obtained at as low as 700 °C. Not only the reaction temperature was lowered, the reaction duration for synthesizing the desired powders was also markedly shortened via the RμE route. The average particle size of the 900 °C-calcined powders was measured to be around 90 nm. The discharge capacities of the prepared o-$LiMnO_2$ powders significantly increased in the initial stages, and rapidly reached a saturated plateau. The impedance spectroscopy analysis revealed that the chemical diffusion coefficient of lithium ions in o-$LiMnO_2$ was markedly greater than that in $LiMn_2O_4$-based materials. The high diffusion rate of lithium ions in o-$LiMnO_2$ is attributed to the high crystallinity as well as the nanosize of the powders synthesized via this RμE process.

Keywords: Electrochemical impedance spectroscopy; Lithium manganese oxide; Lithium-ion batteries; Orthorhombic structure; Reverse-microemulsion process

1. Introduction

Lithium-ion secondary batteries are important power sources for portable electronics, such as laptop computers, cellular phones, and camcorders.[1] In addition, they are also considered as the promising candidates for use in the electric vehicles in the future.[2] $LiCoO_2$ is the primary cathode material in the current generation of commercially available lithium-ion secondary batteries. Due to the high material cost of $LiCoO_2$, many studies have focused on Li–Mn–O-based systems as alternative cathode materials. Lithium manganese oxide compounds are of interest because of their low material cost, high energy density, high working voltage, and acceptable environmental characteristics.[3,4] In the Li–Mn–O system, orthorhombic $LiMnO_2$ (herein abbreviated as o-$LiMnO_2$, space group *Pmmn*, no. 59) with an ordered-rocksalt structure has been considered a promising cathode material in lithium-ion rechargeable batteries.[5–9] The cathodes composed of this material can deliver a specific discharge capacities of 113–272 mAh/g within the voltage range of 2.0–4.5 V at ambient and elevated temperatures.[6,10,11] Orthorhombic $LiMnO_2$, compared with spinel $LiMn_2O_4$, has better discharge characteristics at 3V plateau. In addition, the effects of Jahn-Teller distortion on the structural variation of o-$LiMnO_2$ are hardly noticeable in comparison with the case in spinel $LiMn_2O_4$.[5] Orthorhombic $LiMnO_2$ and monoclinic $LiMnO_2$ are both electrochemically active materials; however, it is difficult to synthesize monoclinic $LiMnO_2$ powders. For obtaining the monoclinic $LiMnO_2$ powders, the heating temperature and the partial pressure of oxygen have to be more strictly controlled.[12–15]

Orthorhombic $LiMnO_2$ is usually synthesized via the conventional solid-state process. For enhancing the diffusivity among solids, the prolonged high-temperature heating is required. However, the heating process will cause severe coarsening of the cathode powders and also

* Corresponding author. Fax: +886-2-3623040.
E-mail address: chlu@ccms.ntu.edu.tw (C.-H. Lu).

0955-2219/03/$ - see front matter © 2003 Elsevier Ltd. All rights reserved.
doi:10.1016/S0955-2219(03)00332-7

cause the volatilization of lithium compounds.[16] Furthermore, the homogeneity of the starting materials is low in the solid-state process and the conversion rate of the chemical reaction will decrease, rendering the stoichiometric deviation in the composition of the heated powders. To overcome the above shortcomings, the macroemulsion process has been developed to synthesize ceramic powders having small particles and a narrow size distribution.[17–20] Nevertheless, the macroemulsion is a thermodynamically metastable system, leading to a rapid phase separation between the aqueous phase and oil phase. A reverse-microemulsion is a type of transparent and thermodynamically stable solution with nanosized water droplets dispersing in the oil phase.[21,22] Once a specific micro-environment is formed; the cations of the starting materials are capable of mixing and interacting in atomic scale to form the desired compounds. In this process, well-mixed microemulsion is utilized to enhance the reactivity of the starting reactants, thereby resulting in the rapid formation of o-$LiMnO_2$ powders at relatively low temperatures.

In this study, a new RμE process has been adopted to synthesize the o-$LiMnO_2$ cathode powders. The effects of oxygen content on the crystal structures of the calcined powders were investigated. The electrochemical characteristics of the synthesized cathode materials were analyzed. The impedance variations related to the formation of the passivation layer and the interparticle contacts in the cathode electrode were also examined.

2. Experimental

Reagent grade lithium nitrate and manganese nitrate were used as the starting materials and individually dissolved in deionized water. The concentrations of lithium-ion solution and manganese-ion solution were both set to 1 M. These solutions were mixed together to form the water phase, and the molar ratio of lithium ions to manganese ions was adjusted to 1.0. The oil phase was composed of cyclohexane using polyoxyethylene (10) octylphenyl ether (OP-10) and *n*-hexyl-alcohol as the surfactant and co-surfactant, respectively. The water phase was well dispersed into the oil phase with a volume ratio of 1:10. A transparent pinkish microemulsion was obtained. The obtained microemulsion was thermodynamically stable. These microemulsions were further heated with various volume ratios of oxygen and argon (herein abbreviated as V_{O_2}/V_{Ar}) at 700–1000 °C. The V_{O_2}/V_{Ar} ratios were adjusted via the volumetric rates of flowing gas in the tube furnace. Powder X-ray diffraction (XRD) was performed to examine the crystal structures of the calcined specimens derived from the RμE process. Scanning electron microscopy (SEM) analyses were carried out to investigate the morphology of the calcined powders. The microstructural morphology and the particle size of orthorhombic $LiMnO_2$ powders were observed by transmission electron microscopy (TEM). Selected area diffraction (SAD) analyses were performed to verify the degree of order in the calcined o-$LiMnO_2$ powders.

For investigating the electrochemical performance of the RμE-derived o-$LiMnO_2$ powders, the cathode electrodes were prepared by mixing the o-$LiMnO_2$ powders, super S carbon black, and polyvinylidene difluoride (PVDF) in a mass ratio of 85:6:9 using N-methyl-2-pyrrolidone (NMP) as the solvent. The slurry was coated onto an Al-foil substrate, followed by heating at 120 °C for 8 h. A lithium foil was adopted as the anode in the cycling test. The electrolyte was comprised of 1 M $LiPF_6$ solution dissolved in a mixture of ethylene carbonate (EC) and dimethyl carbonate (DMC) (1:1 by volume). 2032-type coin cells were assembled in an Ar-filled glove box with moisture less than 1 ppm. The electrochemical studies were galvanostatically performed at a current density of 24.5 mA/g within the voltage range of 2.0–4.5 V at room temperature. Electrochemical impedance spectroscopy (EIS) analyses were performed by applying a DC potential equal to the open circuit of the cell and an AC oscillation of 5 mV in the frequency range from 0.01 to 100 kHz

3. Results and discussion

3.1. Preparation of the RμE-derived o-$LiMnO_2$ powders

The RμE-derived precursors were calcined at 900 °C for 4 h with various V_{O_2}/V_{Ar} ratios. The crystal structures of the calcined powders examined by XRD are illustrated in Fig. 1. It is shown that the calcination atmosphere markedly affected the resulting phases. In pure argon atmosphere, only MnO was obtained. As the oxygen content increased, a minor phase of Mn_3O_4 was formed. Once the V_{O_2}/V_{Ar} ratio increased to 0.02, monophasic o-$LiMnO_2$ was produced without any apparent impurity phase as shown in Fig. 1(c). However, when the V_{O_2}/V_{Ar} ratio reached 0.05, spinel $LiMn_2O_4$ was formed as the major phase and coexisted with a small amount of Mn_3O_4. When the V_{O_2}/V_{Ar} ratio increased to 0.1, the excess oxygen led to an increase in the crystallinity of the spinel phase. The above XRD analyses revealed that the oxygen content in the calcination atmosphere considerably influenced the formed phases and the oxidation states of manganese ions.

The relative amounts of the resultant phases in the clacined specimens are shown in Fig. 2. The relative phase compositions were estimated on the basis of the major diffraction peaks of each compound via the following equation:

$$X_i = \frac{I_i}{\sum I_i} \quad (1)$$

where I_i refers to the diffraction intensity of the major diffraction peak of i-phase, and X_i represents the corresponding phase percentage. As shown in Fig. 2, with a rise in the partial pressure of oxygen, the major phase of the calcined powders varied from MnO to $LiMn_2O_4$. When the V_{O_2}/V_{Ar} ratio was lower than 0.01, the average valence of manganese ions was around 2.0. Increasing the oxygen content in the calcination atmosphere resulted in a rise in the valence of manganese ions. Orthorhombic $LiMnO_2$ powders were obtained as V_{O_2}/V_{Ar} equaled 0.02. Once the V_{O_2}/V_{Ar} ratio was greater than 0.05, the spinel phase became the major component and the corresponding valence of manganese ions was near 3.3. With insufficient oxygen content, the organics in the precursors could not be completely burned out. With an excess oxygen content, the organics burned out completely; however, the valence of manganese ions increased to be larger than 3.0, rendering the mixture of $LiMn_2O_4$ and Mn_3O_4 phases. A previous study also indicated that o-$LiMnO_2$ was formed within a certain oxygen pressure.[9] The above results reveal that the V_{O_2}/V_{Ar} ratio in the calcination atmosphere is a determinant factor in the synthesis of monophasic o-$LiMnO_2$ via the RμE process.

3.2. The temperature effects on the crystallinity evolution of the calcined powders

The XRD patterns of the precursors heated at various temperatures in a $V_{O_2}/V_{Ar} = 0.02$ atmosphere are illustrated in Fig. 3. All the diffraction patterns were characterized to be an orthorhombic structure identical to that reported in the ICDD files.[23] With an increase in the clacination temperature, the crystallinity of the obtained powders increased significantly. The average lattice parameters of the calcined powders were calculated to be $a = 2.8054$ Å, $b = 5.7594$ Å, and $c = 4.5877$ Å, which agreed well with the previous reports.[5,6] In this study, monophasic o-$LiMnO_2$ was formed via the RμE

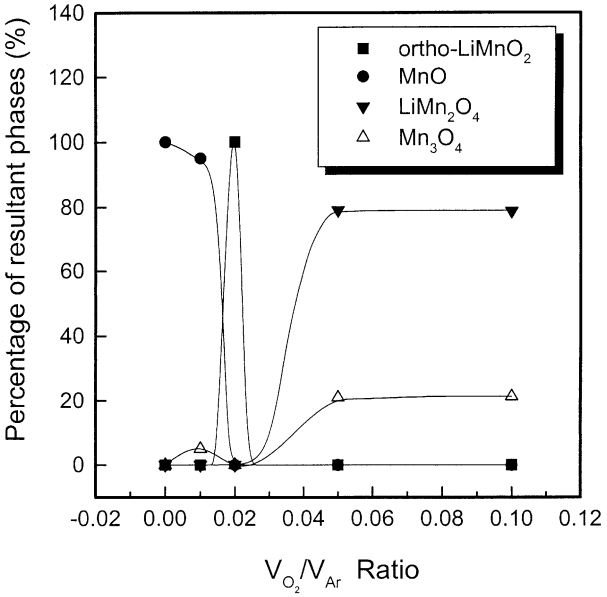

Fig. 2. Relative amounts of the formed phases with various calcination atmospheres in the calcined specimens.

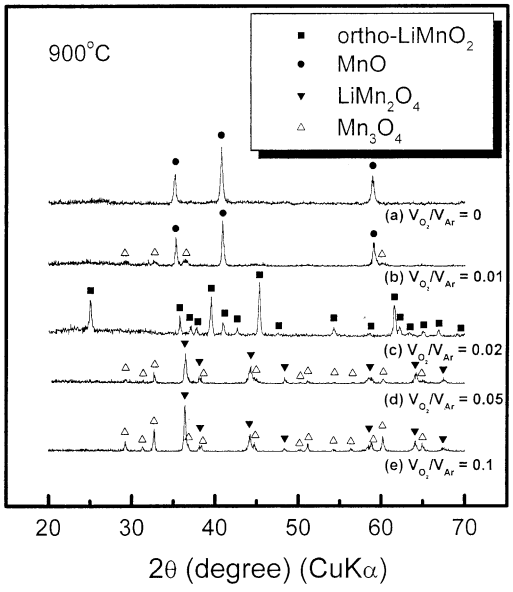

Fig. 1. XRD patterns of the 900 °C-calcined specimens with various calcination atmosphere for 4 h. V_{O_2}/V_{Ar} is (a) 0, (b) 0.01, (c) 0.02, (d) 0.05, and (e) 0.10, respectively.

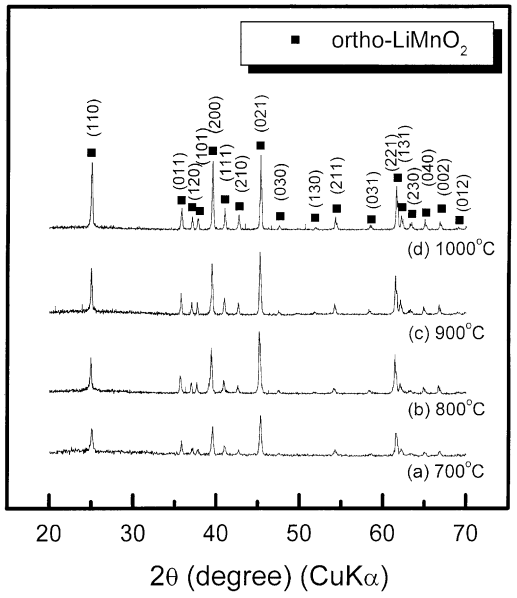

Fig. 3. XRD patterns of the reverse-microemulsion derived powders calcined at (a) 700 °C, (b) 800 °C, (c) 900 °C, and (d) 1000 °C for 4 h.

process after heating the precursors at merely 700 °C. This temperature was markedly lower than that in the traditional solid-state process.[24] In addition, the required clacination duration was notably shortened to 4 h. In the conventional solid-state reaction, more than 10 h was required to prepare o-$LiMnO_2$.[8] This improvement arises from the characteristics of the RμE process. In the initial microemulsion solution, the starting materials were dissolved in the tiny water droplets, which were stabilized by the surfactant and co-surfactant. The size of the micelles in the microemulsion was within a nanometer range, which is beneficial to the mixing of reactants in atomic scale. The special micro-environment can effectively facilitate the chemical reactions so as to lower the calcination temperature and shorten the reaction time.

3.3. The microstructural analyses of o-$LiMnO_2$

Fig. 4 shows the TEM bright field (BF) image and the SAD pattern of the 900 °C-calcined o-$LiMnO_2$. The BF image indicates that the morphology of the calcined powders was angular, where the average particle size was measured to be around 90 nm. The SAD pattern reveals that the prepared powders were single crystallites with good crystallinity. The corresponding zone axis of the SAD pattern was calculated to be $[0\bar{1}1]$. In the solid-state route[5,6,13] and the ion-extraction method,[25] the particle sizes of o-$LiMnO_2$ ranged from 1 to 5 μm. For the RμE-derived powders in this study, the average particle size was significantly reduced to the nanometer range. These powders were fabricated owing to the formation of nanosized reverse micelles.

3.4. Electrochemical characteristics of the RμE-derived o-$LiMnO_2$ powders

In order to achieve good electrochemical performance and acceptable discharge capacity, the 900 °C-calcined powders were utilized as the active materials in the cathode composites. Fig. 5 illustrates the charge and discharge characteristics of the RμE-derived o-$LiMnO_2$ for 30 cycles. It is shown that the first discharge capacity was relatively low. With the cycling preceded, the discharging capacity apparently increased. There were two distinct plateaus in the well-developed discharging trace, representing the electrochemical characteristics of the cycling-induced spinel phase $Li_xMn_2O_4$ formed from o-$LiMnO_2$. For the RμE-derived specimen, the lithium ions inserted into the tetrahedral sites with $0 < x \leqq 1$ at the 4V plateau. The remaining lithium ions inserted into the octahedral sites at the 3V plateau with $1 < x \leqq 2$.[26] In comparison with the spinel $LiMn_2O_4$,[6] the capacity fading of the RμE-derived $LiMnO_2$ cathode was evidently suppressed at 3V plateau. This improved cyclability is ascribed to the improved structural integrity of the cathode materials.[27]

Fig. 6(a) illustrates the characteristics of the specific discharge capacities vs. the cycle number of o-$LiMnO_2$ in the electrochemical test. It was clearly observed that the discharge capacity increased rapidly in the initial cycling stage. After 10 cycles, the steady discharging capacities were achieved at 160 mAh/g. The cathode composite delivered the discharge capacity of 155 mAh/g at the 30th cycle. Fig. 6(b) shows the evolution of discharge capacities of the 3V and 4V plateaus, respectively. It was found that o-$LiMnO_2$ delivered larger discharge

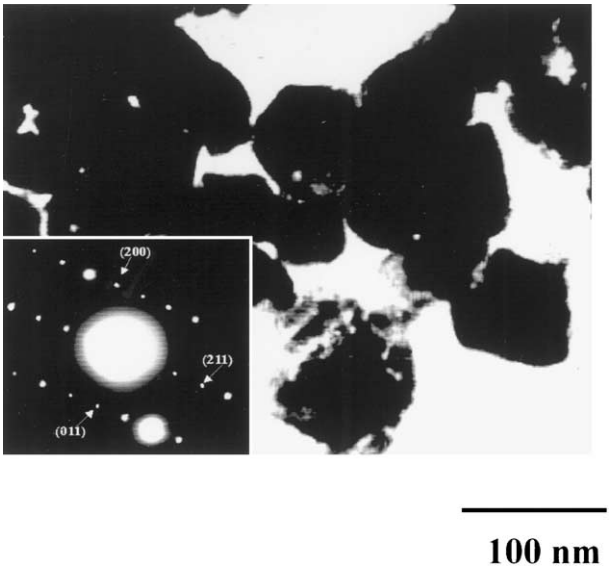

Fig. 4. TEM bright field image of the 900 °C-calcined o-$LiMnO_2$ powders and the corresponding selective area diffraction (SAD) pattern.

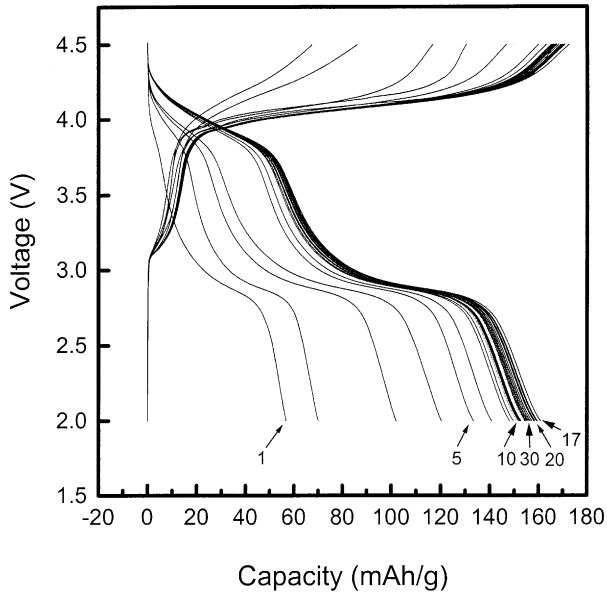

Fig. 5. Charge and discharge characteristics of the RμE-derived o-$LiMnO_2$ for 30 cycles within the voltage range between 4.5 and 2.0 V.

capacities in 3V plateau than 4V plateau. In the previous studies, more than 20 cycles were required for the solid-state-reaction derived o-$LiMnO_2$ to achieve the stable capacities.[28] However, only several cycles were required for the RμE-derived o-$LiMnO_2$ to reach the stable capacity. The required cycle for o-$LiMnO_2$ powders to attain the stable capacity depends on the their particle size.[29] In the RμE process, highly ordered and well crystallized o-$LiMnO_2$ powders were formed, which is advantageous to the intercalation and de-intercalation of lithium ions. In addition, the particle sizes of RμE-derived o-$LiMnO_2$ were small, thereby facilitating the transformation of o-$LiMnO_2$ to the cycling-induced spinel phase $Li_xMn_2O_4$.Therefore, the required cycle to attain the stable capacity of RμE-derived o-$LiMnO_2$ was less than that of the solid-state-reaction derived o-$LiMnO_2$.

The crystal structure of the cycled cathode powders was also examined by XRD. Fig. 7(a) depicts the XRD pattern of uncycled o-$LiMnO_2$ powders. In Fig. 7(b) the specimen after 30 cycles was identified to be the cubic spinel phase. The formation of cycling-induced $Li_xMn_2O_4$ was owing to the phase transformation occurring during cycling.[30] This XRD pattern also revealed the broad width of diffraction peaks after the electrochemical test. The peak broadening was attributed to the creation of local lattice strain and tiny crystallites during cycling. These results were similar to those prepared by the solid-state process.[5]

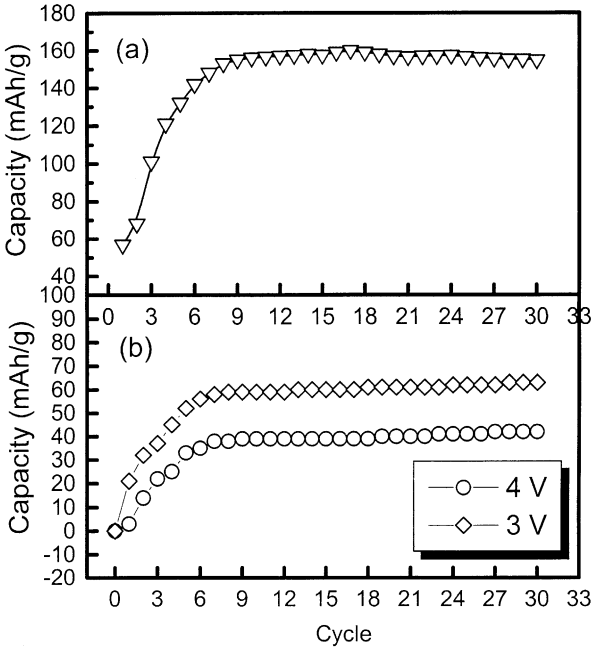

Fig. 6. (a) Characteristics of the specific discharge capacities vs. the cycle number of o-$LiMnO_2$ in the electrochemical test and (b) the evolution of discharge capacities at the 3V and 4V plateaus.

The Nyquist plots of the electrochemical impedance spectroscopy (EIS) analyses are shown in Fig. 8. For the fresh cell, the EIS trace was typically comprised of a semicircle at high frequency and a curve at low frequency region. The semicircle at the high frequency region was related to the solid electrolyte interface (SEI) film of the newly assembled cell. The curve at low frequency region can be explained as the diffusion-controlled process in the electrolytes. After 30 cycles, two overlapped semicircles were observed. The first semicircle at high frequency was relative to the parallel combination of the SEI resistance and its capacitance. The second semicircle at medium frequency was owing to the interaction of the charge transfer resistance (R_{CT}) and the double layer capacitance. In comparison with the EIS curve of the fresh cell, the semicircle of the cycled cell at high frequency was apparently small, which can be attributed to the improvement of ionic conductivity of lithium ions in the SEI film. Once the cell was cycled, the diffusing paths of lithium ions were gradually developed, which enhanced the ionic conductivity, rendering the decreasing in the charge transfer resistance.

The value of the diffusion coefficient, D_{Li}, of lithium ions was calculated via the following equation:[31,32]

$$D_{Li} = \frac{\pi f_i L^2}{1.94} \quad (2)$$

where f_i refers to the frequency of the transition of diffusion from semi-infinite to finite distance, and L is the average particle size of the RμE-derived o-$LiMnO_2$ powders. The chemical diffusion coefficients for the the fresh cell and that after 30 cycles were 3.92×10^{-10} cm^2 s^{-1} and 3.37×10^{-9} cm^2 s^{-1}, respectively. In comparison

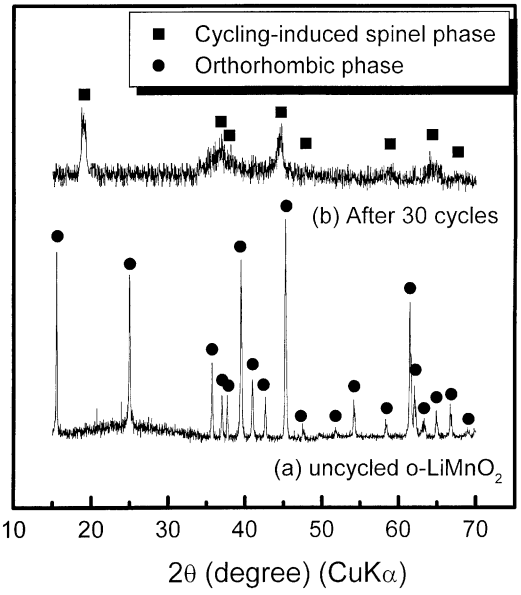

Fig. 7. XRD patterns of (a) uncycled o-$LiMnO_2$ and (b) the cycling-induced spinel powders after 30 cycles.

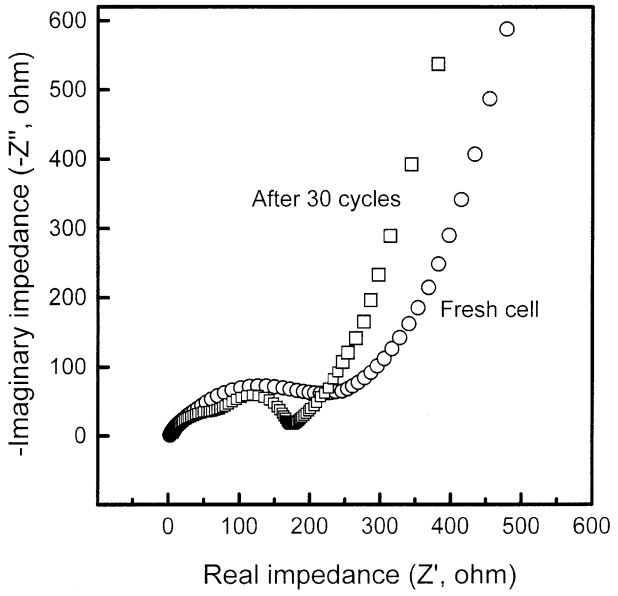

Fig. 8. Electrochemical impedance spectra of the fresh cell and the cell after 30 cycles.

with the EIS analysis of the $LiMn_2O_4$-based materials,[32,33] the diffusion coefficients of lithium ions in this study were markedly larger than those of the doped and undoped $LiMn_2O_4$. The high diffusion rate of lithium ions in o-$LiMnO_2$ is attributed to the high crystallinity as well as the nanosize of the powders synthesized via the RμE process.

4. Conclusions

The RμE technique was successfully developed for synthesizing nanosized orthorhombic $LiMnO_2$ powders in this study. The partial pressure of oxygen had considerable effects on the oxidation states of Mn-ions of the prepared powders. The O_2/Ar volume ratio has to be precisely controlled for synthesizing pure $LiMnO_2$ powders. Monophasic orthorhombic $LiMnO_2$ powders were fabricated after calcining the precursors at 700 °C for only 4 h. In comparison with the conventional solid-state reactions, the required calcination temperature and duration in this study were significantly reduced. The discharge capacities of orthorhombic $LiMnO_2$ gradually increased in the initial stage of the cycling process. The available discharge capacity was measured to be around 160 mAh/g at ambient temperature after 10 cycles. The chemical diffusion coefficient of lithium ions in o-$LiMnO_2$ was markedly larger than that in $LiMn_2O_4$-based materials. The rapid diffusion rate of lithium ions in o-$LiMnO_2$ is ascribed to the high crystallinity and the nanosize of the powders synthesized via this RμE process.

Acknowledgements

The authors would like to thank National Science Council, Taiwan, the Republic of China, for financial support of this study under Contract No. NSC 90-2811-E002-031.

References

1. Thackeray, M. M., Yang, S. H., Kahaian, A. J., Kepler, K. D., Skinner, E., Vaughey, J. T. and Hackney, S. A., Structural fatigue in spinel electrodes in high voltage (4V) $Li/Li_xMn_2O_4$ cells. *Electrochem. Solid-State Lett.*, 1998, **1**, 7–9.
2. Zhang, S. S. and Jow, T. R., Opimization of synthesis condition and electrode fabrication for spinel $LiMn_2O_4$ cathode. *J. Power Sources*, 2002, **109**, 172–177.
3. Xia, Y. and Yoshio, M., Optimization of spinel $Li_{1+x}Mn_{2-y}O_4$ as a 4 V Li-cell cathode in terms of a Li-Mn-O phase diagram. *J. Electrochem. Soc.*, 1997, **144**, 4186–4194.
4. Guyomard, D. and Tarascon, J. M., Li metal-free rechargeable $LiMn_2O_4$/carbon cells: their understanding and optimization. *J. Electrochem. Soc.*, 1992, **139**, 937–948.
5. Cho, J., Kim, T. J. and Park, B., The effects of a metal-oxide coating on the cycling behavior at 55 °C in orthorhombic $LiMnO_2$ cathode materials. *J. Electrochem. Soc.*, 2002, **149**, A288–A292.
6. Lee, Y. S. and Yoshio, M., Preparation of orthorhombic $LiMnO_2$ material by quenching Electrochem. *Solid-State Lett.*, 2001, **4**, A166–A169.
7. Cho, J., Kim, Y. J., Kim, T. J. and Park, B., Enhanced structural stability of o-$LiMnO_2$ by sol-gel coating of Al_2O_3. *Chem. Mater.*, 2001, **13**, 18–20.
8. Wang, G. X., Yao, P., Zhong, S., Bradhurst, D. H. t., Dou, S. X. and Liu, H. K., Electrochemical study on orthorhombic $LiMnO_2$ as cathode in rechargeable lithium batteries. *J. Appl. Electrochem.*, 1999, **29**, 1423–1426.
9. Jang, Y. I. and Chiang, Y. M., Stability of the monoclinic and orthorhombic phases of $LiMnO_2$ with temperature, oxygen partial pressure, and Al doping. *Solid State Ionics*, 2000, **130**, 53–59.
10. Wang, H., Jang, Y. I. and Chiang, Y. M., Origin of cycling stability in monoclinic- and orthorhombic-phase lithium manganese oxide cathodes. *Electrochem. Solid-State Lett.*, 1999, **2**, 490–493.
11. Shu, Z. X., Davidson, I. J., McMillan, R. S. and Murray, J. J., Electrochemistry of $LiMnO_2$ over an extended potential range. *J. Power Sources*, 1997, **68**, 618–622.
12. Jang, Y. I., Moorehead, W. D. and Chiang, Y. M., Synthesis of the monoclinic and orthorhombic phases of $LiMnO_2$ in oxidizing atmosphere. *Solid State Ionics*, 2002, **149**, 201–207.
13. Bruce, P. G., Armstrong, A. R. and Gitzendanner, R. L., New intercalation compounds for lithium batteries: layered $LiMnO_2$. *J. Mater. Chem.*, 1999, **9**, 193–198.
14. Jang, Y., Huang, B., Chiang, Y. M. and Sadoway, D. R., Stabilization of $LiMnO_2$ in the α-$NaFeO_2$ structure type by $LiAlO_2$ addition. *Electrochem. Solid-State Lett.*, 1998, **1**, 13–16.
15. Chiang, Y. M., Sadoway, D. R., Jang, Y., Huang, B. and Wang, H., High capacity, temperature-stable lithium aluminum manganese oxide cathodes for rechargeable batteries. *Electrochem. Solid-State Lett.*, 1999, **2**, 107–110.
16. Li, W. and Currie, J. C., Morphology effects on the electrochemical performance of $LiNi_{1-x}Co_xO_2$. *J. Electrochem. Soc.*, 1997, **144**, 2773–2779.
17. Lu, C. H. and Saha, S. K., Colloid emulsion of nanosized strontium bismith tantalite powder. *J. Am. Ceram. Soc.*, 2000, **83**, 1320–1322.

18. Lu, C. H. and Wang, H. C., Effects of cobat-ion doping on the electrochemical properties of spinel lithium manganese oxide prepared via a reverse-micelle route. *J. Eur. Ceram. Soc.*, 2003, **23**, 865–871.
19. Lu, C. H. and Yeh, P. Y., Ultrafine lithium cobalt oxide powder derived from a water-in-oil emulsion process. *J. Mater. Chem.*, 2000, **10**, 599–601.
20. Lu, C. H. and Lin, S. W., Emulsion-derived lithium manganese oxide powder for positive electrodes in lithium-ion batteries. *J. Power Sources*, 2001, **93**, 14–19.
21. Zarur, A. J. and Ying, J. Y., Reverse microemulsion synthesis of nanostructured complex oxides for catalytic combustion. *Nature*, 2000, **403**, 65–67.
22. Lu, C. H. and Wang, H. C., Synthesis of nanosized $LiNi_{0.8}Co_{0.2}O_2$ derived via a reverse-microemulsion technology. *J. Mater. Chem.*, 2003, **13**, 428–431.
23. *Powder Diffraction File*, Card No. 35–749. International Center for Diffraction Data, Newtown Square, PA.
24. Davidson, I. J., McMillan, R. S., Murray, J. J. and Greedan, J. E., Lithium-ion cell based on orthorhombic $LiMnO_2$. *J. Power Sources*, 1995, **54**, 232–235.
25. Tang, W., Kanoh, H. and Ooi, K., Lithium ion extraction from orthorhombic $LiMnO_2$ in ammonium peroxodisulfate solutions. *J. Solid State Chem.*, 1999, **142**, 19–28.
26. Jang, Y. I., Huang, B., Wang, H., Sadoway, D. R. and Chiang, Y. M., Electrochemical cycling-induced spinel formation in high-charge-capacity orthorhombic $LiMnO_2$. *J. Electrochem. Soc.*, 1999, **146**, 3217–3223.
27. Thackeray, M. M., Structural considerations of layered and spinel lithiated oxides for lithium ion batteries. *J. Electrochem. Soc.*, 1995, **142**, 2558–2563.
28. Croguennec, L., Deniard, P. and Brec, R., Electrochemical cyclability of orthorhombic $LiMnO_2$. *J. Electrochem. Soc.*, 1997, **144**, 3323–3330.
29. Croguennec, L., Deniard, P., Brec, R., Biensan, P. and Broussely, M., Electrochemical behavior of orthorhombic $LiMnO_2$: influence of the grain size and cationic disorder. *Solid State Ionics*, 1996, **89**, 127–137.
30. Koetschau, I., Richard, M. N., Dahn, J. R., Soupart, J. B. and Rousche, J. C., Orthorhombic $LiMnO_2$ as a high capacity cathode for Li-ion cells. *J. Electrochem. Soc.*, 1995, **142**, 2906–2910.
31. Cabanel, R., Barral, G., Diard, J. P., Gorrec, B. L. and Montella, C., Determination of the diffusion coefficient of an inserted species by impedance spectroscopy: application to the $H/H_xNb_2O_5$ system. *J. Appl. Electrochem.*, 1993, **23**, 93–97.
32. Myung, S. T., Komaba, S. and Kumagai, N., Enhanced structural stability and cyclability of Al-doped $LiMn_2O_4$ spinel synthesized by the emulsion drying method. *J. Electrochem. Soc., 148, A482-A489.*, 2001.
33. Zhang, S. S., Jow, T. R., Amine, K. and Heriksen, G. L., $LiPF_6$-EC-DMC electrolyte for Li-ion battery. *J. Power Sources*, 2002, **107**, 18–23.